Behaviors of beryllium compensation doping in InGaAsP grown by gas source molecular beam epitaxy

Y. J. Ma, Y. G. Zhang, Y. Gu, S. P. Xi, X. Y. Chen, Baolai Liang, Bor-Chau Juang, Diana L. Huffaker, B. Du, X. M. Shao, and J. X. Fang

Citation: AIP Advances **7**, 075117 (2017);

View online: https://doi.org/10.1063/1.4989884

View Table of Contents: http://aip.scitation.org/toc/adv/7/7

Published by the American Institute of Physics

Behaviors of beryllium compensation doping in InGaAsP grown by gas source molecular beam epitaxy

Y. J. Ma,[1] Y. G. Zhang,[1,a] Y. Gu,[1] S. P. Xi,[1] X. Y. Chen,[1] Baolai Liang,[2] Bor-Chau Juang,[2] Diana L. Huffaker,[2] B. Du,[1] X. M. Shao,[3] and J. X. Fang[3]
[1]*State Key Laboratory of Functional Materials for Informatics, Shanghai Institute of Microsystem and Information Technology, Chinese Academy of Sciences, Shanghai 200050, China*
[2]*Department of Electrical Engineering, University of California, Los Angeles, CA 90095, U.S.A.*
[3]*Key Laboratory of Infrared Imaging Materials and Devices, Shanghai Institute of Technical Physics, Chinese Academy of Sciences, Shanghai 200083, China*

(Received 8 May 2017; accepted 17 July 2017; published online 27 July 2017)

We report structural properties as well as electrical and optical behaviors of beryllium (Be)-doped InGaAsP lattice-matched to InP grown by gas source molecular beam epitaxy. P type layers present a high degree of compensation on the order of 10^{18} cm^{-3}, and for Be densities below 9.5×10^{17} cm^{-3}, they are found to be n type. Enhanced incorporation of oxygen during Be doping is observed by secondary ion mass spectroscopy. Be in forms of interstitial donors or donor-like Be-O complexes for cell temperatures below 800°C is proposed to account for such anomalous compensation behaviors. A constant photoluminescence energy of 0.98 eV without any Moss-Burstein shift for Be doping levels up to 10^{18} cm^{-3} along with increased emission intensity due to passivation effect of Be is also observed. An increasing number of minority carriers tend to relax via Be defect state-related Shockley-Read-Hall recombination with the increase of Be doping density. [http://dx.doi.org/10.1063/1.4989884]

I. INTRODUCTION

Compensation doping in compound semiconductors and the associated carrier transport and recombination dynamics are of great importance for device designs and analyses, especially when p type light doping is of concern. $In_xGa_{1-x}As_yP_{1-y}$ quaternary alloys (referred to as InGaAsP hereafter) lattice-matched to InP substrates, with wide tunable band gaps in the wavelength range between 0.9 and 1.7 μm and high electron mobilities, play an important role in industry for light emitting diodes, lasers, detectors, solar cells, bipolar transistors and modulators. Specifically, by fine tailoring of the cutoff wavelength, InGaAsP single-photon avalanche photodiodes can offer much enhanced detection efficiency at 1064 nm and lower dark count rate compared with InGaAs ones, which is of vital importance for 1.06 μm light imaging detection and ranging.[1]

P type InGaAsP alloys play important roles in diverse pn junction devices such as the light absorbers in electron-initiated avalanche photodiodes,[2] the p-side waveguides in laser diodes,[3] the 1.0 eV absorber in tandem solar cells,[4] and the base layer in heterojunction bipolar transistors,[5] for which the carrier relaxation properties of InGaAsP dramatically affects the device performances. Due to the fact that undoped epitaxial InGaAsP appears natively n type, inverting the doping polarity is technically realized in compensated regimes using acceptors of beryllium (Be), magnesium and zinc. The residual dopant atoms in gas source molecular beam epitaxy systems, e.g. silicon (Si), oxygen (O), hydrogen (H), carbon (C) and sulphur (S), normally act as n type background dopants during growth of InGaAs-InP materials, which renders the atomic process of Be compensation doping more

[a]Electronic mail: ygzhang@mail.sim.ac.cn

complicated. Further, it has been shown that incorporation of O via formation of Be-O complexes could occur in the growth of Be-doped InGaAs, leading to an increased degree of compensation and enhanced impurity scattering.[6,7] In order to uncover the carrier relaxation dynamics in InGaAsP alloys, considerable efforts have been devoted to the optical and lifetime characterizations of bulk and quantum well type structures thus far.[4,6,8–14] However, only very few have addressed p type InGaAsP[4,14] where compensation behaviors become of major concern. A comprehensively understanding on the carrier transport and relaxation behaviors in p type InGaAsP, especially at different Be compensation degrees, is still of great significance to device applications.

We report results from structural, carrier transport and detailed recombination studies on compensation doped InGaAsP as a function of Be density, including x-ray diffraction (XRD), secondary ion mass spectroscopy (SIMS), Hall transport, transmission spectroscopy, and steady-state and time-resolved photoluminescence (PL), from which we show that p type layers present an anomalously high degree of compensation on the order of 10^{18} cm^{-3}, and incorporation of oxygen is enhanced during Be doping.

II. MATERIALS GROWTH

Epitaxial InGaAsP layers were lattice-matched grown on Fe-doped semi-insulating (100) InP with a resistivity of $\rho = 2 \times 10^7\ \Omega \cdot$cm by a VG Semicon-V80H gas-source molecular beam epitaxy (GSMBE). The background pressure is less than 10^{-10} Torr. The growth was carried out at a substrate temperature of 520°C under pressures typically in the range of 10^{-5} Torr. Si and Be were used as n and p dopants in this system, respectively. Unintentionally doped InGaAsP is n type with a low carrier concentration around 1×10^{16} cm^{-3} and a relatively high mobility of ~3000 cm^2/Vs at room temperature (RT). Five 0.6-μm-thick InGaAsP samples with Be cell temperatures varying from 735°C, 760°C, 780°C, 800°C and 830°C were grown at a same growth rate of 1.0 μm/h. The corresponding Be densities (N_{Be}), measured by SIMS, are from 1.3×10^{17} to 1.9×10^{18} cm^{-3}. Table I lists the measured primary physical parameters of these five samples (referred to as B735, B760, B780, B800 and B830, respectively). 2×1 surface reconstruction reflection high-energy electron diffraction (RHEED) patterns were clearly observed during the growth, indicating good crystallinity of the InGaAsP films. In order to realize p type lightly-doped InGaAsP, we implemented modulation doping by repeatedly opening and closing the Be shutter for 2 and 8 s, respectively, during growth of B830. The interlayer diffusion and redistribution of Be atoms between modulation doped layers as well as the high diffusivity of Be in InGaAs-InP material system[15] was expected to give rise to an overall light p type doping.

III. RESULTS AND DISCUSSION

A. X-ray diffraction

XRD measurements were performed first to evaluate the crystal lattice information for these Be-doped InGaAsP alloys. Figure 1 shows the normalized double crystal (004) XRD rocking curves. All five samples show small lattice mismatches of less than ±400 arcseconds with respect to InP substrate and strong peak intensities for InGaAsP layers. While consistently tensile strain is found for

TABLE I. Measured primary physical parameters of the InGaAsP samples at different Be cell temperatures. The minus and positive signs for Hall N_A refer to the n and p type conductivities, respectively.

Sample	Be cell T (°C)	SIMS N_{Be} (cm^{-3})	SIMS N_O (cm^{-3})	Hall N_A (cm^{-3})	Hall mobility (cm^2/Vs)	300 K τ_{ave} (ps)
B735	735	1.3×10^{17}	7.9×10^{16}	-2.9×10^{16}	203.1	317.0
B760	760	3.9×10^{17}	1.2×10^{17}	-1.7×10^{17}	111.3	212.7
B780	780	9.5×10^{17}	1.0×10^{17}	-4.4×10^{17}	71.8	192.6
B800	800	1.9×10^{18}	1.0×10^{17}	$+3.3\times10^{18}$	28.2	146.2
B830	830	1.2×10^{18}	3.0×10^{16}	$+2.3\times10^{18}$	31.4	112.8

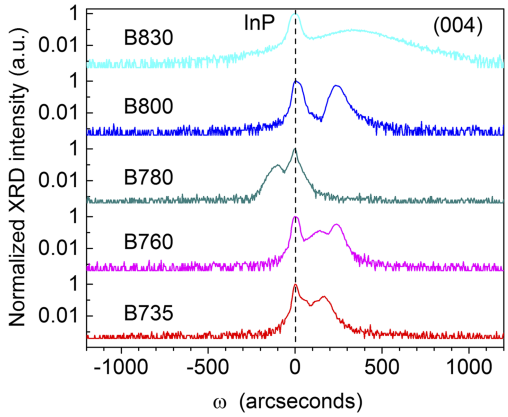

FIG. 1. Normalized (004) XRD rocking curves for the InGaAsP/InP wafers at different Be cell temperatures.

the other four ones, B780 appears to be compressively strained, probably caused by the composition fluctuation during growth but not the Be cell temperature differences. More detailed alloy composition information for these quaternary layers cannot be accurately determined from figure 1 due to the coexistence of two group V elements. Unlike uniform doped samples of B735, B760, B780 and B800 with relatively sharp InGaAsP peaks, the modulation-doped B830 exhibits a much broader InGaAsP envelope with full width at half maximum of over 300 arcseconds. Such degraded lattice ordering could result from the increased alloy distortion generated by excessive high density of Be interstitial or substitutional impurities.

B. Secondary ion mass spectroscopy

Depth profiles of Be, O, H, C, S and Si atom concentrations for these samples were obtained from SIMS analyses. Figure 2(a) shows the profiles for B780. The measured atom concentrations of Si, H, C, S are all below the detection limits, which are 4×10^{14}, 2×10^{16}, 2×10^{15} and 1×10^{14} cm^{-3}, respectively. The peaks near the InGaAsP surface and the InGaAsP/InP interface are not real, due to mass interferences. Figure 2(b) plots the extracted atom concentrations for Be and O as a function of Be cell temperature. It is seen that N_{Be} linearly increases with Be cell temperature from 735°C to 800°C, while for modulation doped B830 the mean N_{Be} is 1.2×10^{18} cm^{-3}, roughly equals to 1/5 of its linearly extrapolated value assuming uniform doping. This percentage is also in good agreement

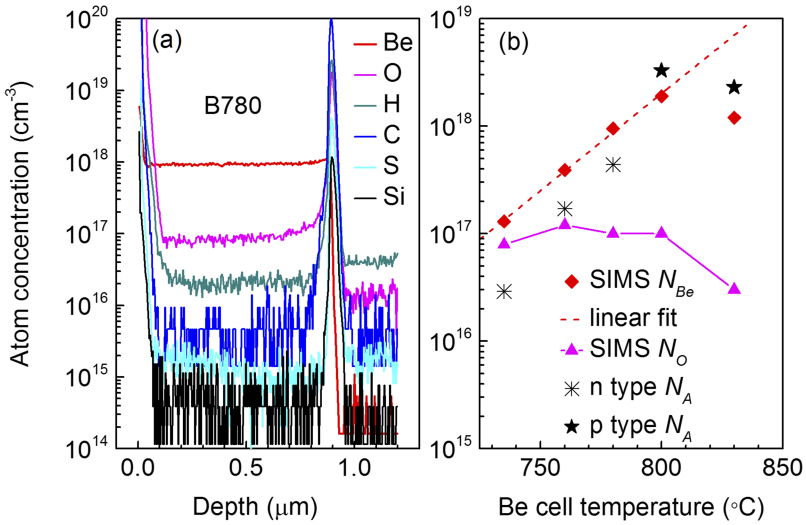

FIG. 2. (a) SIMS depth profiles of Be, O, H, C, S and Si atom concentrations in B780. (b) Extracted atom concentrations for Be and O as well as the measured Hall N_A as a function of Be cell temperature. Red dash line is a linear fitting for N_{Be}.

with the modulated shutter duration of opening 2 s and closing 8 s for Be cell, indicating modulation doping of Be could be an effective route towards control and lowering the p type concentration. O was found to incorporate with a high concentration (N_O) around 1×10^{17} cm^{-3} from B735 to B800. N_O first increases from 7.9×10^{16} cm^{-3} for B735 to 1.2×10^{17} cm^{-3} for B760, and then saturates at around 1×10^{17} cm^{-3} for Be cell temperatures up to 800°C. For B830 with Be shutter opened for 1/5 of the total thickness, O incorporation is largely reduced to 3×10^{16} cm^{-3}, clearly demonstrates the incorporation of O in InGaAsP is enhanced during Be doping.

C. Hall transport

Free carrier concentrations (N_A) measured by Hall effect at RT are also plotted in figure 2(b) as a function of Be cell temperature (also listed in Table I). For N_{Be} from 1.3×10^{17} to 9.5×10^{17} cm^{-3}, all samples behaved as n type, with an anomalous increasing trend of Hall N_A from 2.9×10^{16} to 4.4×10^{17} cm^{-3}. For N_{Be} above 1×10^{18} cm^{-3}, samples invert to p type. The Hall concentration of modulation-doped B830 is 2.3×10^{18} cm^{-3}, roughly close to 1/3 of the linearly extrapolated N_{Be} at the Be cell temperature of 830°C. Hall mobilities decrease from 203.1 to 71.8 cm^2/Vs with Be density for n type samples, and then remain ~30 cm^2/Vs for p type B800 and B830. The measured electron mobilities for the n type samples are more than one order of magnitude lower than that for the unintentionally doped n type InGaAsP grown by this GSMBE system and other previously reported n type InGaAsP,[16] suggesting that the carrier scattering therein is significantly enhanced. Therefore, it is reasonable to infer that a large portion of Be would behave as interstitial dopants for B735, B765 and B780, which ionize to increase the electron density on the one hand, and on the other hand, enhance the carrier scattering. For B800 and B830 with further increased Be densities, the mobility values are on the same orders of magnitude with the reported hole mobilities in p-type InGaAsP lattice-matched to InP[16] with Be densities from 10^{16} to 10^{20} cm^{-3}, indicating most Be became substitutional and took the group III atom positions. Given the enhanced incorporation of O during Be doping, interstitial Be in these InGaAsP layers may also exist as donor-like Be-O complexes which has been observed in Be-doped InGaAs[7] grown by solid source MBE. Formation of Be-O complexes could also account for the inhibition of the substituting behaviors of Be for group III atoms for $N_{Be} \leq 1 \times 10^{18}$ cm^{-3} and the associated high degree of compensation.

Post-growth thermal annealing treatments up to 60 min were also performed at 340°C for these Be-doped samples under forming gas ambience. Neither doping polarity conversion nor noteworthy carrier concentration or mobility changes were observed after annealing, demonstrating again the Be atoms therein have already been activated, i.e. ionized or bonded.

D. Optical transmission

Figure 3 shows the RT light absorption spectra for the five Be-doped InGaAsP layers measured by using an optical transmission method in a fourier transform infrared spectrometer. The absorption

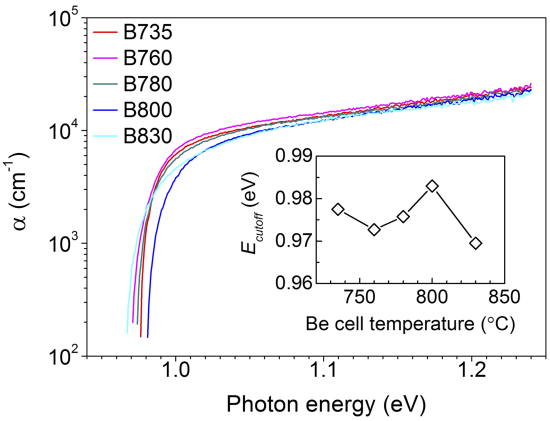

FIG. 3. Measured RT light absorption spectra for the five Be-doped InGaAsP layers. Inset: E_{cutoff} as a function of Be cell temperature.

coefficients, α, are almost the same for all five sample for photon energies above 1.1 eV. For photons with energies between 1.1 eV and the cutoff energies (E_{cutoff}), the p type samples of B800 and B830 exhibit slightly reduced α while the other three n type samples still retain almost the same. The E_{cutoff}, as shown by the inset of figure 3, slightly blue shifts to 982 meV for B800 and then red shifts to 970 meV for B830, with a mean value of 976±6 meV. Such small shifts of E_{cutoff} for InGaAsP with different Be doping could be caused by the slight alloy composition fluctuation as observed in XRD measurements (figure 1). The frequently observed large Moss-Burstein shifts[17–19] due to degenerate carrier distribution in heavily doped semiconductors is not found here, indicating the band structure is not considerably affected by Be compensation doping.

E. Steady-state photoluminescence

Steady-state 300 K PL spectra for the samples excited by a 532 nm continuous wave semiconductor laser at a power density of 2 W/cm^2 are shown in figure 4(a). The energy resolution of the monochromator in our PL setup is 0.5-1 meV (depends on the wavelength). Strong PL emissions at around the same peak energy of 978 meV (978±3 meV) were observed for all five InGaAsP layers (figure 4(b)), well consistent with the E_{cutoff} obtained from the transmission measurements (figure 3). The slightly red shift of peak energy to 975 meV for B780 is related to the exceptionally compressive strain as measured by XRD. The integrated PL intensity (I_{PL}) first increases with increasing the Be cell temperature from 735-780°C and then steeply drops after p type conversion, as shown in figure 4(c). Such an increment from B735 to B780 suggests an increasing number of inherent non-radiative recombination centers, such as point defects or vacancies, are passivated by the interstitial Be or Be-O complexes. For B800 and B830, most Be atoms became substitutional and therefore such passivation effects are removed, the PL intensities drop to levels close to that of B735. In addition, the PL peak energies for all five samples are independent on excitation powers for laser power densities up to 2.5 W/cm^2. These PL results again verify the unaffected band structure of InGaAsP with Be doping densities up to 1.9×10^{18} cm^{-3}.

Figures 5(a)–(c) show the temperature-dependent PL spectra for B735, B800 and B830 over 77-300 K, respectively. B780 and B800 revealed similar temperature-dependent spectra to B735 and thus are not shown. The PL intensities dramatically increase with decreasing temperature for all five samples while the PL energies blue shift to higher values following a fitted Varshni relation of

$$E_g(T) = \frac{1.04 - (6.54 \times 10^{-4} T^2)}{633.32 + T} \quad (1)$$

in unit of eV, where T is temperature and $E_g(T)$ is PL energy. A small envelope with emission energy slightly lower than that of the InGaAsP appears for all samples at 77 K, which is also shown separately in figure 5(d) for the 77 K PL spectrum of B780. By fitting with two Gaussian functions,

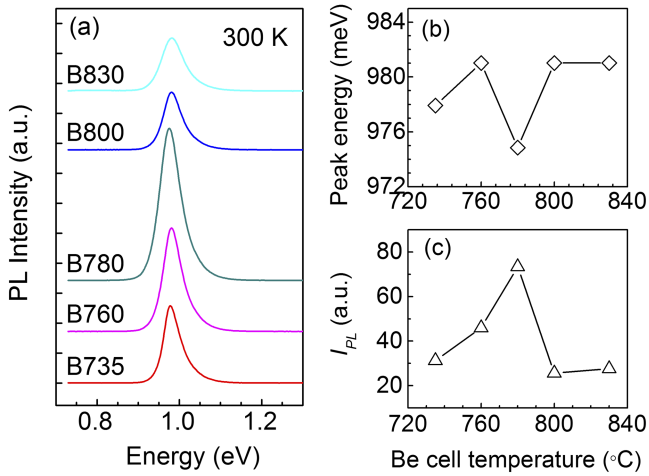

FIG. 4. (a) 300 K PL spectra for the five InGaAsP samples excited by a same laser power density of 2 W/cm^2. (b) PL peak energy and (c) integrated PL intensity (I_{PL}) as a function of Be cell temperature.

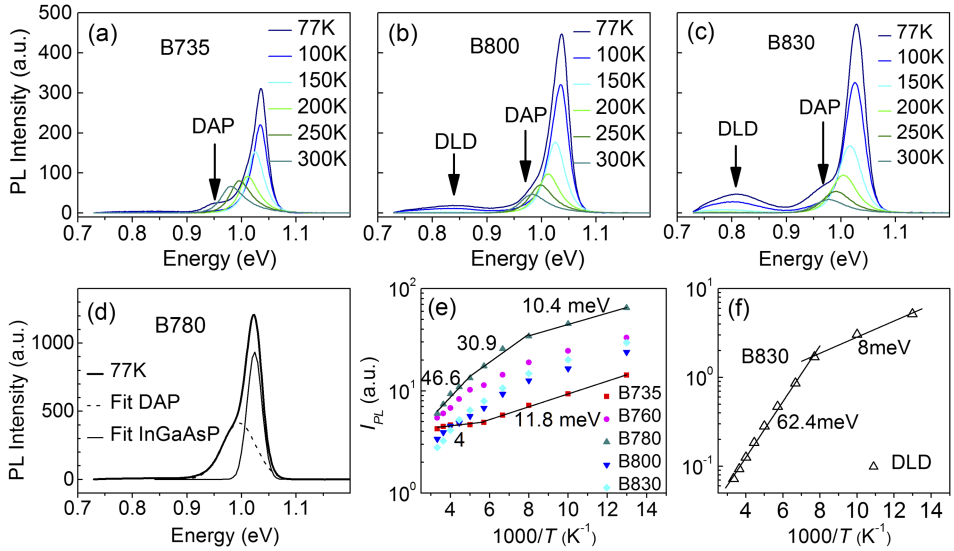

FIG. 5. (a)-(c) Temperature-dependent PL spectra for B735, B800 and B830, respectively. (d) 77 K PL spectrum of B780 and the decomposed subpeaks from DAP and InGaAsP. (e) and (f) Arrhenius plots of I_{PL} for the InGaAsP peaks of all samples and for the DLD peaks of B830, respectively. The fitted E_a at different temperature ranges are indicated.

a strong PL peak at 1023.7 meV and a weak PL peak at 995.3 meV are obtained. The previous one is from the band edge emission of InGaAsP while the latter one is attributed to be luminescence from the donor-acceptor pair (DAP) excitons.[20] In addition, another broad PL envelope around 0.8 eV becomes increasingly observable at Be density over 10^{18} cm^{-3} and blue shifts with decreasing temperature (figures 5(b) and (c)). This envelope originates from the deep-level defect (DLD) bands induced by substitutional Be atoms at excess high Be doping levels. DLDs act not only as radiative recombination centers but as carrier traps within the band gap.[6] Activation energies (E_a) are extracted from these PL data to further identify the peak origins. Figures 5(e) and (f) show the Arrhenius plots of I_{PL} for the InGaAsP peaks of all samples and for the DLD peaks of B830, respectively. I_{PL} follows linear dependences on $1000/T$ with varied slopes at different temperature ranges, which can be fitted using the relation of

$$I_{PL} = \frac{I_0}{1 + \mathrm{A}\exp\left(-\frac{E_a}{k_B T}\right)} \tag{2}$$

where I_0 is the I_{PL} at absolute zero, A is a fitting parameter related to the nonradiative recombination centers, and k_B is the Boltzmann constant. The extracted E_a from figure 5(e) are listed in Table II. E_a for B735 is 11.8 meV at 77-175 K and decreases to 4 meV at 175-300 K, which match with the ionization energies of shallow Si donors observed in III-V alloys.[21] The other four samples reveal very approximate E_a at the same temperature ranges, which are ~11, ~25 and ~40 meV at 77-125, 125-225 and 225-300 K, respectively, matching with the ionization energies of Be acceptors.[21] Also noteworthy is that B735 exhibits a much slower increase of I_{PL} with decreasing temperature in comparison to

TABLE II. Extracted E_a from I_{PL} for the InGaAsP peaks of all samples at different temperature ranges.

Sample	77-175 K (meV)	175-300 K (meV)	
B735	11.8	4.0	
Sample	77-125 K (meV)	125-225 K (meV)	225-300 K (meV)
B760	9.6	19.3	32.7
B780	10.4	30.9	46.6
B800	11.0	23.5	37.7
B830	12.2	25.0	49.2

the other four samples, suggesting the Be passivation effect for non-radiative recombination centers became more evident at lower temperatures. E_a obtained from figure 5(f) are 8 and 62.4 meV at 77-250 and 250-300 K, respectively, which are attributed to the detrapping energies of the DLDs. The alloy composition is accordingly determined to be $In_{0.74}Ga_{0.26}As_{0.55}P_{0.45}$ from the 300 K optical band gap of 978 meV and the shallow Be acceptor energy level of 40 meV, assuming a perfect lattice match.

F. Photoluminescence lifetimes

Carrier relaxation dynamics are investigated by time-resolved PL (TRPL) measurements. The samples were excited by 5 ps pulses at 26 MHz from a NKT Photonics SuperK Extreme laser running at 633 nm, with an average excitation power of ~0.5 W/cm^2. The luminescence was dispersed in a spectrometer and detected with a Hamamatsu H10330-75 near-IR photomultiplier tube (PMT). The decay signals were collected by a PicoHarp-300 time correlated single photon counting (TCSPC) module. All TRPL decays were acquired by setting the monochromator at corresponding peak PL wavelengths. The system time resolution is about 50 ps by using deconvolution fitting.

Figure 6(a) shows the 300 K TRPL decay curves of the five samples. The luminescence decays are not single exponentials, and vary considerably for different Be doping densities. The measurement artefacts close to 3-4 ns are due to structure in the tail of the instrument response function (IRF) of the PMT, as also shown in figure 6(a). These decay curves are best fitted using a tri-exponential relation of

$$I(t) = A_0 + A_1 e^{-t/\tau_1} + A_2 e^{-t/\tau_2} + A_3 e^{-t/\tau_3} \quad (3)$$

where t is time, $I(t)$ is the counted PL intensity, A_0, A_1, A_2 and A_3 are fitting parameters, τ_1, τ_2, and τ_3 are lifetimes correspond to the initially fast and the followed two slow decays, as clearly shown in figure 6(b) for the 300 K decay curve of B735. The fitted three lifetimes and the corresponding amplitudes are listed in Table III. The time taken for the luminescence intensity to fall to 1/e of its initial value is characterized by the average lifetime τ_{ave} calculated by $\tau_{ave}=\Sigma A_i\tau_i/\Sigma A_i$, which monotonically decreases with increasing Be cell temperature, as shown in figure 6(c). Such a lifetime trend suggests an increasing number of non-equilibrium carriers tend to relax via Be-related defect states that monotonically increases with Be cell temperature.

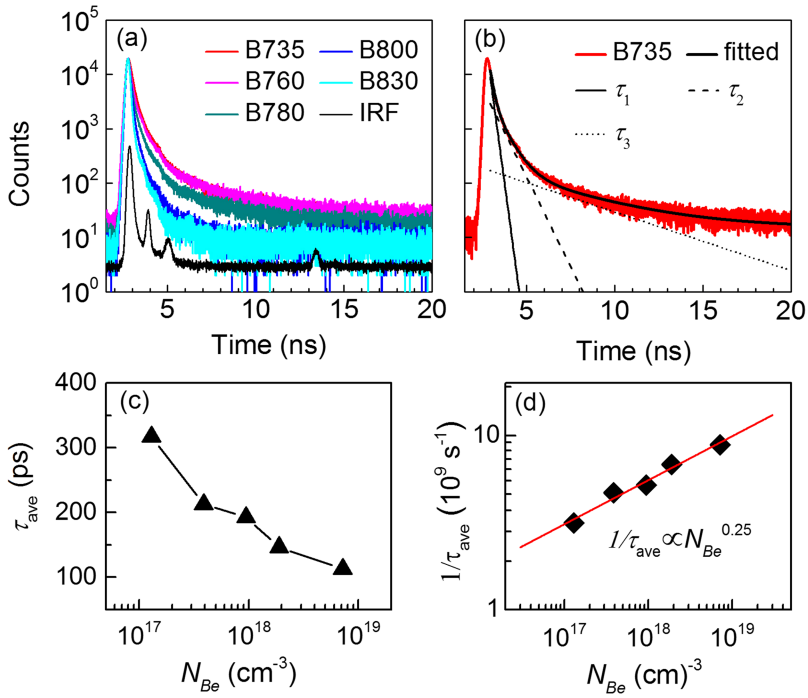

FIG. 6. (a) 300 K TRPL decay curves for the five samples. The IRF of the PMT detector is also shown. (b) Tri-exponential fitting results for the 300 K decay curve of B735. (c) The extracted τ_{ave} as a function of N_{Be}. (d) $1/\tau_{ave}$ plotted as a function of N_{Be}. The line is a linear fitting.

TABLE III. The fitted three lifetimes and the corresponding amplitudes for the 300 K TRPL decay curves of the five samples shown in figure 6(a).

	τ_1 (ps)	A_1	τ_2 (ps)	A_2	τ_3 (ps)	A_3
B735	180.5±0.5	12826.5	659.0±4.4	3246.0	4.0±0.07	172.4
B760	125.3±0.4	29070.7	532.7±2.4	5495.2	3.9±0.06	211.5
B780	108.1±0.3	17051.4	429.4±2.3	3992.9	3.0±0.05	174.8
B800	97.2±0.3	10557.7	347.5±4.2	1866.1	1.7±0.07	91.2
B830	64.4±0.9	6590.5	137.6±8	1549.1	0.5±0.0007	691.1

In general, the measured lifetime of the sample can be described by[22,23]

$$\frac{1}{\tau_{meas}} = \frac{1}{\tau_{SRH}} + \frac{1}{\tau_{Rad}} + \frac{1}{\tau_{Auger}} + \frac{1}{\tau_{surf}} \tag{4}$$

where τ_{SRH}, τ_{Rad}, τ_{Auger} and τ_{surf} are the Shockley-Read-Hall (SRH), radiative, Auger and surface recombination lifetimes, respectively. Under low or intermediate injection condition ($\Delta n \ll N_{Be}$, where Δn is the injected minority density), τ_{meas} can be further described in terms of N_{Be} by

$$\frac{1}{\tau_{meas}} = \frac{1}{\tau_{SRH}} + BN_{Be} + CN_{Be}^2 + \frac{2S}{d} \tag{5}$$

where B and C are radiative and Auger recombination coefficients, respectively. S is the surface recombination velocity and d is the film thickness. However, since S is related to surface states and insensitive to Be doping, τ_{surf} can be approximately treated as a constant for these five samples. Note that equation (5) is derived theoretically from a consideration of minority carrier decay for pure p or n type semiconductors, taking N_{Be} as the majority carrier density might not be fully rigorous when compensation doping occurs. However, since the measured Hall concentration follows exactly the same trend as N_{Be} in these InGaAsP layers (see figure 2(b)), we suggest this equation would also represent a reasonable approximation for modeling the carrier relaxation in these compensation doped samples. We plot $1/\tau_{ave}$ as a function of N_{Be}, as shown in figure 6(d). A linear fitting gives a relation of $1/\tau_{ave} \propto {N_{Be}}^{0.25}$ which coincides with neither radiative ($1/\tau_{Rad} \propto N_{Be}$) nor Auger ($1/\tau_{Aug} \propto {N_{Be}}^2$) dependences.[24] Thereby, we suggest the defect state-related SRH recombination plays an increasing role with the increase of Be doping density. Note the SRH defects involved here are Be-related trap states but not mid gap centers since these lattice-matched InGaAsP layers have quite good crystal quality. In addition, excitation power-dependent TRPL measurements were also performed for all five samples (not shown), showing lifetimes independent on the excitation laser power of our setup. The absence of saturation effects of lifetimes at high excitation powers further verifies the reasonability of above attribution.

Also we should point out that the nonradiative decay rate at large N_{Be} could be underestimated by using the fitted relationship of $1/\tau_{ave} \propto {N_{Be}}^{0.25}$. By comparing with the lifetimes of 1-10 ns reported in lightly-doped p type InGaAsP,[4] the measured overall short lifetimes in these unpassivated samples are likely dominated by recombination at the unpinned InGaAsP/air interfaces.

Figure 7(a) shows the temperature-dependent TRPL decay curves of B735 over 77-300 K. The lifetime declines with lowering the temperature. Figures 7(b) shows the extracted τ_{ave} as a function of temperature for all five samples. τ_{ave} increases consistently with increasing temperature for all five samples, while B735 exhibits a much larger τ_{ave} in the range of 90-350 ps compared to the other four samples with τ_{ave} ranging from 50 to 160 ps. Such positive temperature coefficients for these highly compensated InGaAsP layers are in stark contrast to the negative temperature coefficients that are frequently reported in lattice-matched n type semiconductor films, such as $In_{0.53}Ga_{0.47}As$ bulk film,[19] InAs/GaSb and InAs/$InAs_{0.72}Sb_{0.28}$ superlattices.[25,26] Furthermore, trends of increase followed by decrease at 77-300 K are also reported in n type InAs/$InAs_{0.72}Sb_{0.28}$ superlattice and HgCdTe due to competitive relaxation via different channels.[27–29]

In terms of temperature, the SRH, Auger and radiative lifetimes can be described by Refs. 25–28,30 τ_{SRH}=$P_1 T^{-1/2}$, τ_{Rad}=$P_2 T^{3/2}$, and $\tau_{Auger} = P_3 (\frac{E_g}{k_B T})^{3/2} \exp(\frac{1+2\mu}{1+\mu} \cdot \frac{E_g}{k_B T})$, respectively, where P1, P2 and P3 are fitting parameters, E_g is the temperature-dependent band gap energy expressed by

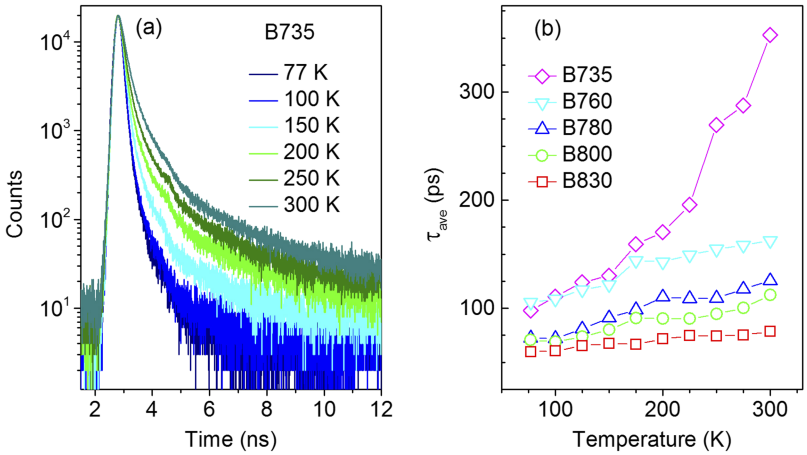

FIG. 7. (a) Temperature-dependent TRPL decay curves for B735. (b) The extracted temperature-dependent τ_{ave} for the five samples.

equation (1), $\mu = m_e/m_h$, m_e and m_h are the electron and hole effective masses, respectively. The fitting of the temperature-dependent τ_{ave} using equation (4) does not converge when only the above three components are considered, which indicates that surface recombination could play an important role in the relaxation process. In essential, τ_{ave} are results of competitive relaxation among the four channels. If the surface recombination velocities at the InGaAsP/InP and InGaAsP/air interfaces are large and not strongly temperature dependent, then as the sample temperature is lowered, an increase in the diffusion coefficient as the temperature is decreased will cause more carriers to preferentially recombine at both interfaces, leading to reduced τ_{ave} at lower temperatures.

In the meantime, from figures 7(b), the decreasing trend of τ_{ave} with increasing N_{Be} at 300 K (figure 6(c)) remains unchanged over the whole measured temperature range. Moreover, the temperature coefficient of τ_{ave} also monotonically decreases with increasing Be doping density. These characteristics demonstrate again that the non-radiative SRH recombination becomes increasingly pronounced at higher Be cell temperatures.

IV. CONCLUSIONS

In conclusion, we have performed comprehensively structural, electrical and optical characterizations for Be compensation doped InGaAsP as a function of Be density. High degree of compensation on the order of 10^{18} cm^{-3} is observed for p type layers, while for N_{Be} below 1×10^{18} cm^{-3} samples behave as n type. Enhanced incorporation of O during Be doping is observed by SIMS analyses. Be in forms of interstitial donors or donor-like Be-O complexes for cell temperatures below 800°C is proposed to elucidate such anomalous compensation behaviors. A constant photoluminescence energy of 0.98 eV without any Moss-Burstein shift for Be doping levels up to 10^{18} cm^{-3}, along with increased emission intensity due to passivation effects of Be is also observed. An increasing number of non-equilibrium carriers are identified to relax via Be defect state-related SRH recombination with the increase of Be doping density. These advances serve as important references for device designers and material fabricators involving p type InGaAsP, and also for other compensation doped III-V quaternary alloys.

ACKNOWLEDGMENTS

We gratefully acknowledge financial support from the following sources: National Key Research and Development Program of China (No. 2016YFB0402400), the National Natural Science Foundation of China (Nos. 61605232, 61675225 and 61405232), Youth Innovation Promotion Association CAS (No. 2013155), the Shanghai Sailing Program (No. 15YF1414300), and the Open Program of Key Laboratory of Infrared Imaging Materials and Detectors (No. IIMDKFJJ-15-08).

[1] X. Jiang, M. A. Itzler, R. Ben-Michael, and K. Slomkowski, IEEE J Sel. Top. Quant. **13**, 895 (2007).
[2] J. P. Donnelly, E. K. Duerr, K. A. Mcintosh, E. A. Dauler, D. C. Oakley, S. H. Groves, C. J. Vineis, L. J. Mahoney, K. M. Molvar, P. I. Hopman, K. E. Jensen, G. M. Smith, S. Verghese, and D. C. Shaver, IEEE J. Quantum Elect. **42**, 797 (2006).
[3] Y. Y. Cao, Y. G. Zhang, Y. Gu, X. Y. Chen, and L. Zhou, IEEE Photonic. Tech. L. **26**, 571 (2014).
[4] L. Ji, S.-L. Lu, Y.-Y. Wu, P. Dai, L.-F. Bian, M. Arimochi, T. Watanabe, N. Asaka, M. Uemura, A. Tackeuchi, S. Uchida, and H. Yang, Sol. Energ. Mat. Sol. C. **127**, 1 (2014).
[5] N. Shamir, D. Ritter, and C. Cytermann, Solid State Electron. **42**, 2039 (1998).
[6] L. Qian, S. D. Benjamin, P. W. E. Smith, B. J. Robinson, and D. A. Thompson, Appl. Phys. Lett. **71**, 1513 (1997).
[7] A. L. Corre, J. Caulet, M. Gauneau, S. Loualiche, H. L'Haridon, D. Lecrosnier, A. Roizes, and J. P. David, Appl. Phys. Lett. **51**, 1597 (1987).
[8] B. Sermage, H. J. Eichler, J. P. Heritage, R. J. Nelson, and N. K. Dutta, Appl. Phys. Lett. **42**, 259 (1983).
[9] B. Sermage, J. P. Heritage, and N. K. Dutta, J. Appl. Phys. **57**, 5443 (1985).
[10] E. Wintner and E. P. Ippen, Appl. Phys. Lett. **44**, 999 (1984).
[11] A. M. Fox, R. J. Manning, and A. Miller, J. Appl. Phys. **65**, 4287 (1989).
[12] J. M. Smith, G. S. Buller, D. Marshall, A. Miller, and C. C. Button, Appl. Phys. Lett. **80**, 1870 (2002).
[13] S. Juodkazis, M. Petrauskas, A. Quacha, and M. Willander, Phys. Status Solidi A **140**, 439 (1993).
[14] W.-X. Yang, L. Ji, P. Dai, M. Tan, Y.-Y. Wu, J.-Y. Lu, B.-J. Li, J. Gu, S.-L. Lu, and Z.-Q. Ma, Acta Phys. Sin.-CH ED **64**, 177802 (2015).
[15] T. Mozume and K. Hosomi, J. Cryst. Growth **175/176**, 1223 (1997).
[16] K. Tappura, J. Appl. Phys. **74**, 4565 (1993).
[17] M. P. Lumb, M. K. Yakes, M. Gonzalez, J. G. Tischler, and R. J. Walters, J. Appl. Phys. **114**, 103504 (2013).
[18] Z. M. Gibbs, A. LaLonde, and G. J. Snyder, New J. Phys. **15**, 075020 (2013).
[19] Y. J. Ma, Y. Gu, Y. G. Zhang, X. Y. Chen, S. P. Xi, Z. Boldizsar, L. Huang, and L. Zhou, J. Mater. Chem. C **3**, 2872 (2015).
[20] T. H. Gfroerer, C. E. Gillespie, J. P. Campbell, and M. W. Wanlass, J. Appl. Phys. **98**, 093708 (2005).
[21] Y. A. Goldberg and N. M. Schmidt, "Handbook series on semiconductor parameters," (World Scientific, London, 1999) pp. 153–179.
[22] R. K. Ahrenkiel, R. Elling, S. Johnston, and M. Wanlass, Appl. Phys. Lett. **72**, 3470 (1998).
[23] R. K. Ahrenkiel, S. W. Johnston, J. D. Webb, L. M. Gedvilas, and J. J. Carapella, Appl. Phys. Lett. **78**, 1092 (2001).
[24] D. Vignaud, J. F. Lampin, E. Lefebvre, M. Zaknoune, and F. Mollot, Appl. Phys. Lett. **80**, 4151 (2002).
[25] B. C. Connelly, G. D. Metcalfe, H. Shen, and M. Wraback, Appl. Phys. Lett. **95**, 251117 (2010).
[26] E. H. Steenbergen, B. C. Connelly, G. D. Metcalfe, H. Shen, M. Wraback, D. Lubyshev, Y. Qiu, J. M. Fastenau, A. W. K. Liu, S. Elhamri, O. O. Cellek, and Y.-H. Zhang, Appl. Phys. Lett. **99**, 251110 (2011).
[27] L. Höglund, D. Z. Ting, A. Khoshakhlagh, A. Soibel, C. J. Hill, A. Fisher, S. Keo, and S. D. Gunapala, Appl. Phys. Lett. **103**, 221908 (2013).
[28] B. V. Olson, E. A. Shaner, J. K. Kim, J. F. Klem, S. D. Hawkins, M. E. Flatté, and T. F. Boggess, Appl. Phys. Lett. **103**, 052106 (2013).
[29] Y. Chang, C. H. Grein, J. Zhao, C. R. Becker, M. E. Flatte, P.-K. Liao, F. Aqariden, and S. Sivananthan, Appl. Phys. Lett. **93**, 192111 (2008).
[30] B. V. Olson, E. A. Shaner, J. K. Kim, J. F. Klem, S. D. Hawkins, L. M. Murray, J. P. Prineas, M. E. Flatté, and T. F. Boggess, Appl. Phys. Lett. **101**, 092109 (2012).